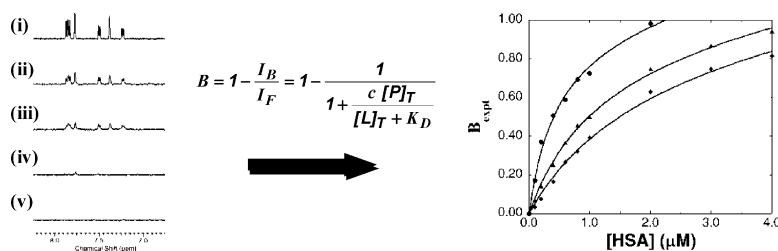


## Estimating Protein#Ligand Binding Affinity Using High-Throughput Screening by NMR

Matthew D. Shortridge, David S. Hage, Gerard S. Harbison, and Robert Powers

*J. Comb. Chem.*, **2008**, 10 (6), 948-958 • DOI: 10.1021/cc800122m • Publication Date (Web): 03 October 2008

Downloaded from <http://pubs.acs.org> on November 17, 2008



### More About This Article

Additional resources and features associated with this article are available within the HTML version:

- Supporting Information
- Access to high resolution figures
- Links to articles and content related to this article
- Copyright permission to reproduce figures and/or text from this article

[View the Full Text HTML](#)

# Estimating Protein–Ligand Binding Affinity Using High-Throughput Screening by NMR

Matthew D. Shortridge, David S. Hage, Gerard S. Harbison, and Robert Powers\*

Department of Chemistry, University of Nebraska, Lincoln, Nebraska 68588

Received July 14, 2008

Many of today's drug discovery programs use high-throughput screening methods that rely on quick evaluations of protein activity to rank potential chemical leads. By monitoring biologically relevant protein–ligand interactions, NMR can provide a means to validate these discovery leads and to optimize the drug discovery process. NMR-based screens typically use a change in chemical shift or line width to detect a protein–ligand interaction. However, the relatively low throughput of current NMR screens and their high demand on sample requirements generally makes it impractical to collect complete binding curves to measure the affinity for each compound in a large and diverse chemical library. As a result, NMR ligand screens are typically limited to identifying candidates that bind to a protein and do not give any estimate of the binding affinity. To address this issue, a methodology has been developed to rank binding affinities for ligands based on NMR screens that use 1D  $^1\text{H}$  NMR line-broadening experiments. This method was demonstrated by using it to estimate the dissociation equilibrium constants for twelve ligands with the protein human serum albumin (HSA). The results were found to give good agreement with previous affinities that have been reported for these same ligands with HSA.

## Introduction

Over the past decade, nuclear magnetic resonance (NMR) spectroscopy has evolved as an important tool for drug discovery.<sup>1</sup> Current NMR screening methods complement structural biology efforts by validation of chemical leads from high-throughput screening (HTS) prior to initiation of a structure-based drug design program.<sup>2–7</sup> The first NMR screening methods, such as SAR by NMR,<sup>4</sup> RAMPED-UP NMR,<sup>8</sup> and NMR-SOLVE,<sup>9</sup> were developed to identify ligands that bind a therapeutic target in a biologically relevant manner by observing chemical shift changes in two-dimensional (2D)  $^1\text{H}$ – $^{15}\text{N}$  HSQC spectra. However, these methods tend to be resource-intensive. Their relatively low throughput also makes it impractical to use these methods for collecting complete binding curves that allow binding affinities (often represented by the dissociation equilibrium constant,  $K_{\text{D}}$ ) to be measured as an integral component of an NMR screen. To overcome these issues, recent methods, such as MS/NMR<sup>10</sup> and multistep NMR screening,<sup>11</sup> have applied a tiered approach to screening that joins complementary techniques to increase throughput and minimize resource usage. For instance, the multistep NMR screen combines one-dimensional (1D)  $^1\text{H}$  NMR line-broadening experiments and 2D  $^1\text{H}$ – $^{15}\text{N}$  HSQC chemical shift perturbation experiments to identify drug discovery leads from a biologically relevant, small-molecule library.<sup>12</sup>

Ligand-focused 1D NMR methods are well suited to identify hits from large chemical libraries because they favor weak-affinity ligands (i.e., ligands with  $K_{\text{D}}$  values in the range

of micro to millimolar quantities), decrease data-collection time, and reduce overall sample requirements.<sup>7</sup> In addition, with the advent of sample changers and flow-probes, ligand-focused 1D NMR experiments can be readily adapted to automation to give a corresponding increase in throughput.<sup>7,13–17</sup> A number of fast, ligand-focused 1D NMR experiments exist that exploit differences in relaxation rates, diffusion rates, saturation transfers, or NOE transfers to identify protein–ligand complexes.<sup>3,18</sup> In general, a binding event is identified by using a change in line width or chemical shift in the free ligand 1D- $^1\text{H}$  NMR spectrum upon the addition of a protein. However, using these measurements to determine the dissociation equilibrium constant for a protein–ligand complex as part of an NMR screen is still a challenging task.<sup>19–25</sup>

Similar to traditional measurements,<sup>20</sup> NMR methods rely on the collection of multiple data points to accurately determine a dissociation equilibrium constant or binding affinity for a protein–ligand interaction.<sup>9</sup> This approach is usually impractical in a high-throughput mode that requires a rapid method for characterizing and ranking binding affinities. Examples of single-point  $K_{\text{D}}$  measurements using 1D NMR experiments have recently been described that use  $^{19}\text{F}$ -containing compounds<sup>21,22</sup> or the displacement of known low-affinity inhibitors.<sup>24,26</sup> Unfortunately, these approaches are typically limited in practice because known low-affinity inhibitors or a large library of druglike and structurally diverse  $^{19}\text{F}$ -containing compounds are not available for a wide range of protein targets.

This report discusses a new NMR screening method that can be used to determine the relative ranking of binding affinities using a variation of traditional 1D  $^1\text{H}$  NMR line-broadening experiments.<sup>27,28</sup> This approach correlates the

\* To whom correspondence should be addressed. Phone: (402) 472-3073. Fax (402) 472-9402. E-mail: rpowers3@unl.edu.

ratio of NMR peak height for free and bound ligands to the fraction of bound ligand in a protein–ligand complex. This method is illustrated by using human serum albumin (HSA) as a model protein, which is an important secondary target for efficacy screening and a well-established system for monitoring protein–ligand interactions.<sup>29</sup>

### Theory

Binding interactions between a large protein (MW > 5000 Da) and a low molecular weight ligand (MW < 500 Da) can be examined by using the decrease in NMR peak height that occurs upon the addition of a protein to a solution with a constant ligand concentration. NMR line-broadening experiments follow an opposite protocol from typical experiments that measure  $K_D$  values, where ligands are added to solutions that contain a constant protein concentration. Thus, a different form for the standard Langmuir binding isotherm is required in the former type of study. If it is assumed that a protein (P) has a 1:1 binding with a ligand (L), the dissociation equilibrium constant for this interaction can be represented by the following equation:

$$K_D = \frac{[L]_F[P]_F}{[PL]} \quad (1)$$

where  $[P]_F$  is the concentration of the free protein at equilibrium,  $[L]_F$  is the corresponding concentration of the free ligand, and  $[PL]$  is the concentration of the resulting protein–ligand complex.

Rearrangement of eq 1 produces the following binding isotherm, in which  $f_B$  represents the “fractional occupancy” or the fraction of bound ligand.

$$f_B = \frac{[PL]}{[L]_T} = \frac{1}{1 + \frac{K_D}{[P]_F}} \quad (2)$$

It is assumed in many types of binding studies that the total ligand concentration  $[L]_T$  is approximately equal to the free ligand concentration; however, this assumption is not applicable to the NMR line-broadening experiments used in this study because  $[L]_T$  is not necessarily in excess of the maximum complex concentration  $[PL]$ . Also, a direct measurement of the free protein concentration is not possible for the method described in this report. Therefore, eq 3 was derived to describe this situation in terms of the total protein concentration  $[P]_T$  and total ligand concentration  $[L]_T$  that are known to be present in the system (see Appendix for derivation).

$$f_B = \frac{[PL]}{[L]_T} = \frac{1}{1 + \frac{2K_D}{([P]_T - [L]_T - K_D) + \sqrt{([P]_T - [L]_T + K_D)^2 + 4K_D[L]_T}}} \quad (3)$$

Equation 3 can be simplified to approximate the fractional occupancy in terms of the total ligand concentration  $[L]_T$  and total protein concentration  $[P]_T$  by using a Taylor series expansion and the assumption that  $[L]_T > [P]_T$ .

$$f_B = \frac{[PL]}{[L]_T} \approx \frac{[P]_T}{([L]_T + K_D)} \quad (4)$$

The fractional occupancy for a protein–ligand complex can be measured using a ratio of NMR peak height ( $1 - I_B/I_F$ ), where  $I_B$  is the sum of ligand NMR peak heights in the presence of the protein and  $I_F$  is the sum of NMR peak heights for the free ligand. Therefore,  $B$  (the NMR peak height ratio) represents an easily measurable response of ligand binding that can be described in terms of the fraction of bound ligand ( $f_B$ ) and the NMR-line width for the free ( $\nu_F$ ) and bound ( $\nu_B$ ) states (see Appendix for derivation).

$$B = 1 - \frac{I_B}{I_F} = 1 - \frac{1}{1 + f_B \left( \frac{\nu_B}{\nu_F} - 1 \right)} \quad (5)$$

Combination of eq 4 and eq 5 leads to a new binding isotherm for this system, as shown below:

$$B = 1 - \frac{I_B}{I_F} = 1 - \frac{1}{1 + \frac{c[P]_T}{[L]_T + K_D}} \quad \text{where } c = \frac{\nu_B}{\nu_F} - 1 \quad (6)$$

The unitless NMR-line width ratio constant ( $c$ ), as defined in eq 6, accounts for the proportional change in ligand line width upon binding of a ligand to a protein. Once a ligand is bound, the free ligand line width ( $\nu_F$ ) of a ligand resonance adopts the line width of the protein ( $\nu_B$ ), and the increase in line width produces a corresponding decrease in peak height measured by the ratio of NMR peak height ( $B$ ).

The dissociation equilibrium constant for a protein–ligand complex that is calculated using eq 6 is based on relative changes in NMR peak height by fitting the given binding isotherm to a complete protein titration curve. This is impractical in the context of an NMR high-throughput screen, where only a single titration point is measured. However, eq 6 can be rearranged to solve for  $K_D$  to yield an estimate for  $K_D$  that is based on  $[P]_T$ ,  $[L]_T$ ,  $c$ , and  $B_{\text{single}}$ , where  $B_{\text{single}}$  is the fractional occupancy at a single protein concentration. The resulting expression is shown in eq 7.

$$K_D = \left[ \left( \frac{c[P]_T}{B_{\text{single}}} - c[P]_T \right) - [L]_T \right] \quad (7)$$

For proteins, such as HSA, that possess multiple nonspecific binding sites, the decrease in ligand signal at a relatively high protein concentration will be an average of specific and nonspecific binding. To correct for this effect, the nonspecific binding term  $n[P]_T$  that corresponds to a linear increase in fraction bound with the addition of protein is simply added to eq 6, as shown in eq 8.

$$B = 1 - \frac{I_B}{I_F} = 1 - \frac{1}{1 + \frac{c[P]_T}{[L]_T + K_D}} + n[P]_T \quad (8)$$

### Experimental Section

**Materials.** The HSA (essentially fatty acid free,  $\geq 96\%$  pure), choline bromide ( $\sim 99\%$  pure), clofibrate, furosemide, phenol red, phenylbutazone, phenytoin ( $\sim 99\%$  pure), sodium

salicylate, tolbutamide, uridine 5'-monophosphate (98–100% pure), and warfarin (>98% pure) were purchased from Sigma (St. Louis, MO). The bromophenol blue (ACS reagent grade, 95% pure), bromocresol green (ACS reagent grade, 95% pure), and ibuprofen were from Sigma-Aldrich (Milwaukee, WI). The dimethyl sulfoxide- $d_6$  (99.9% D), deuterium oxide (99.9% D), and naproxen (98% pure) were obtained from Aldrich (Milwaukee, WI). The 3-(trimethylsilyl)propionic-2,2,3,3- $d_4$  acid sodium salt (98% D) was purchased from Cambridge Isotope (Andover, MA). The potassium phosphate dibasic salt (anhydrous, 99.1% pure) and monobasic salt (crystal, 99.8% pure) were purchased from Mallinckrodt (Phillipsburg, NJ).

**Apparatus.** All NMR spectra were collected on a Bruker 500 MHz Avance spectrometer (Billerica, MA) equipped with a triple-resonance, Z-axis gradient cryoprobe and using a Bruker BACS-120 sample changer and IconNMR software for automated data collection. Spectra were collected at 298 K using 512 transients, a sweep-width of 6009 Hz, 16 K data points, and a relaxation delay of 2.0 s. The residual HDO resonance signal was suppressed with presaturation. The total experiment time, including sample changing for each spectrum, was approximately 33 min.

**Sample Preparation.** All small-molecule ligands that were used in this study were selected based on their previously reported  $K_D$  values for HSA and their good solubility in an aqueous solution.<sup>29</sup> The small-molecule ligand samples were individually prepared in 10 mL stock solutions that contained 20  $\mu\text{M}$  ligand, 1% (v/v) dimethyl sulfoxide- $d_6$  (DMSO- $d_6$ ), 10  $\mu\text{M}$  3-(trimethylsilyl)propionic-2,2,3,3- $d_4$  acid sodium salt (TSP), and pH 7.0 (uncorrected) 50 mM potassium phosphate buffer prepared in deuterium oxide.

A series of ten HSA stock solutions were prepared in deuterium oxide by making serial dilutions from a 200  $\mu\text{M}$  master solution of HSA in deuterium oxide. The final concentrations of HSA in these stock solutions ranged from 0 to 200  $\mu\text{M}$  and were prepared so that a 10  $\mu\text{L}$  addition of the HSA stock solution to 490  $\mu\text{L}$  of a free ligand solution resulted in final concentrations of 0, 0.1, 0.2, 0.4, 0.6, 0.8, 1, 2, 3, and 4  $\mu\text{M}$  HSA, respectively. These mixtures were prepared individually for each ligand in 1.5 mL microcentrifuge tubes and then transferred to NMR tubes. The sample for each titration that contained 0  $\mu\text{M}$  HSA was used as the reference for calculation of the free ligand intensities ( $I_F$ ) and free ligand linewidths ( $\nu_F$ ). All binding studies performed with these solutions were conducted at 25  $^\circ\text{C}$ .

**1D  $^1\text{H}$  NMR Binding Curves.** Spectra were processed with the ACD/1D NMR manager (Advanced Chemistry Development, Inc., Toronto, Ontario). A linear prediction algorithm was applied to the FID in the forward direction and the resulting FID was Fourier transformed. The NMR spectrum was phase-adjusted and baseline-corrected. The residual water signal was removed for clarity using the solvent removal function in ACD. This function simply sets the spectrum's baseline to zero around the residual water signal. All ligand resonance peaks were visually selected and peak positions were measured relative to a TSP reference set to 0.0 ppm. Peak heights were measured relative to the DMSO- $d_6$  peak at 2.69 ppm that was normalized to a height

of 1.00. The DMSO- $d_6$  peak was completely recovered during the 1D  $^1\text{H}$  NMR experiment using a 2.0 s recycle delay, which is  $>3 \times$  the  $T_1$  for DMSO in  $\text{D}_2\text{O}$  at 299 K (0.3–0.5 s).<sup>30,31</sup> Individual peak heights in the aromatic region for each ligand were summed to obtain the free ( $I_F$ ) and bound ( $I_B$ ) heights at each titration point. The peak height ratios were plotted versus total protein concentration and fit to eq 8 using the program KaleidaGraph version 3.52 for Windows (Synergy Software., Reading, PA) to estimate the  $K_D$  value for each protein–ligand complex. The average NMR-line width ratio ( $c$ ) for each ligand was estimated by using eq 6, where  $\nu_B$  was taken to be approximately 94.2 Hz using a previously measured correlation time for HSA of 41 ns.<sup>32</sup> The value for  $\nu_F$  was calculated as described in the next section. The fit of each binding curve was constrained so that  $K_D \geq 0$  in these studies.

**Measuring a Free Ligand NMR Line Width ( $\nu_F$ ).** To measure the free ligand line width ( $\nu_F$ ) for use in eq 6, the NMR spectrum for each free ligand (i.e., as obtained in a solution containing no HSA) was processed as described above to avoid any distortion in line width resulting from processing. NMR peak line widths were measured using the ACD/1D NMR manager peak fitting routine. The average peak line width was used to report  $\nu_F$  for each ligand and to calculate the NMR line width ratio.

**Simulated High-Throughput Screening by NMR.** To simulate the outcome of an NMR high-throughput screening assay, a single protein concentration  $[\text{P}]_T$  from the full titration curve was used. On average, the 0.2  $\mu\text{M}$  HSA titration point yielded a large response for all 12 ligands without reaching saturation. The static total ligand concentration  $[\text{L}]_T$  was 20  $\mu\text{M}$ . A simulated response curve was generated by fitting a range of  $K_D$  values to a range of ideal  $B_{\text{single}}$  values calculated using eq 7. The measured  $B_{\text{single}}$  value for each ligand at the 0.2  $\mu\text{M}$  HSA titration point was used to calculate a single-point binding constant from eq 7 and compared to the simulated response curve. This simulated experiment used both the individual  $c$  values calculated for each ligand from the full titration experiment and an average  $c$  value calculated from the 12 NMR titration curves. The single-point dissociation equilibrium constant for each ligand was calculated using this average  $c$  value.

## Results and Discussion

**Measuring  $K_D$  from 1D  $^1\text{H}$  NMR Line-Broadening Experiments.** The development of NMR-based screening assays that monitor changes in chemical shifts or line width as a means to identify or verify initial chemical leads has evolved to become an increasingly important component of drug discovery efforts in the biotechnology and pharmaceutical industry.<sup>33,34</sup> Nevertheless, the direct measurement of a binding affinity from a high-throughput NMR screen is generally lacking.<sup>21–25</sup> A decrease in the height of a ligand's NMR signal in the presence of a protein is commonly used in NMR-based screens to monitor the formation of a protein–ligand complex. The 1D  $^1\text{H}$  NMR spectra of small-molecules (MW  $\leq$  500 Da) usually have extremely sharp peaks because of the slow dipole–dipole relaxation ( $T_2$ ).<sup>3</sup> Binding to a high molecular weight agent, like a protein,

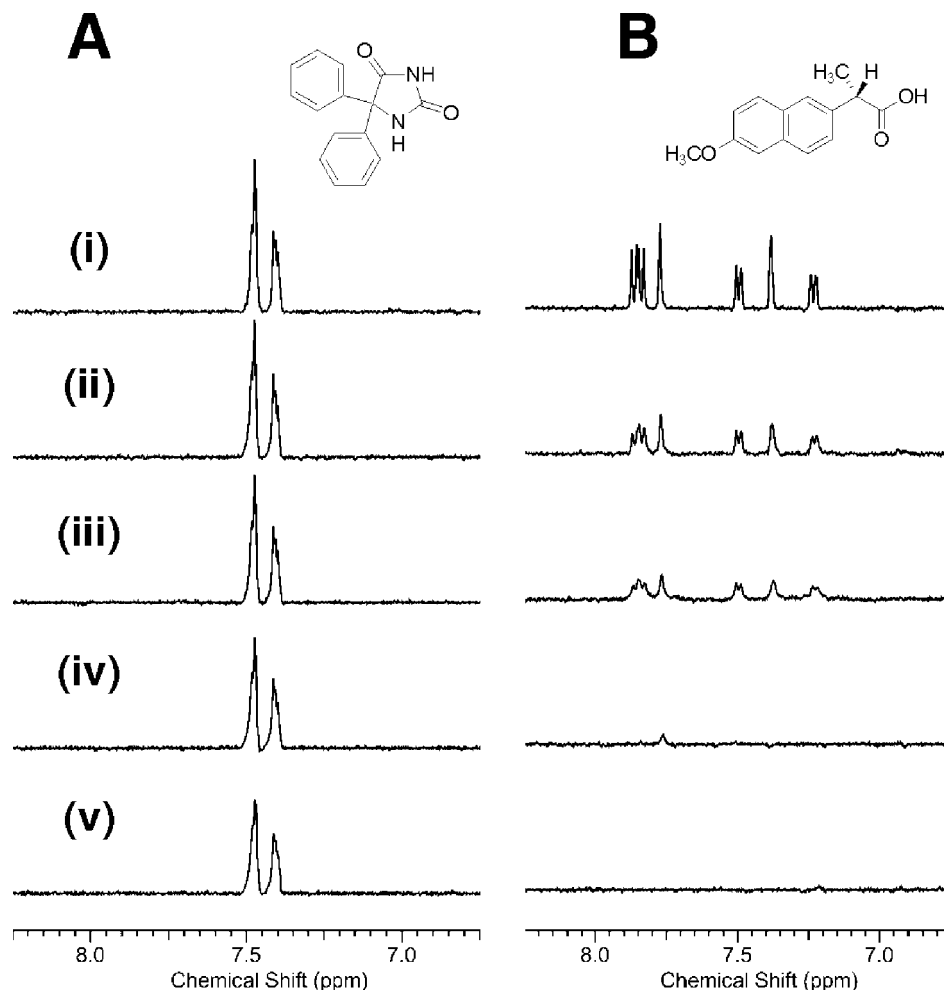


**Figure 1.** 1D  $^1\text{H}$  NMR spectra for titration of 20  $\mu\text{M}$  solutions of the drugs phenytoin (A) and naproxen (B) with increasing concentrations of HSA. The concentrations of HSA were as follows: (i) 0, (ii) 0.4, (iii) 1, (iv) 2, and (v) 4  $\mu\text{M}$ . As the protein concentration increases, the height of the ligand NMR signal decreases because the bound ligand adopts the shorter relaxation time of the protein. The decrease in the ratio of NMR signal height ( $I_{\text{B}}/I_{\text{F}} - 1$ ) is proportional to the degree of binding, such that tighter binding ligands will relax more quickly than weaker binding ligands. This relationship provides an estimate of the dissociation constant for a protein–ligand complex.

induces peak broadening and a corresponding decrease in the ligand's NMR signal height because the bound ligand now experiences the shorter relaxation time of the protein. This effect is illustrated in Figure 1 using binding by the protein HSA to the drugs phenytoin and naproxen as examples.

The observed increase in ligand line width in such an experiment will depend on a number of factors that include the dissociation equilibrium constant for the protein–ligand interaction,  $K_{\text{D}}$ . In general, the observed change in the ligand's line width ( $\nu_{\text{obs}}$ ) for the fast exchange limit will follow the result shown below.

$$\nu_{\text{obs}} = \nu_{\text{F}} + f_{\text{B}}(\nu_{\text{B}} - \nu_{\text{F}}) \quad \text{where } f_{\text{B}} \approx \frac{[\text{P}]_{\text{T}}}{[\text{L}]_{\text{T}} + K_{\text{D}}} \quad (9)$$

In eq 9,  $f_{\text{B}}$  is the fraction of the bound protein–ligand complex,  $\nu_{\text{F}}$  is the free ligand NMR line width, and  $\nu_{\text{B}}$  is the line width for the bound state of the ligand (see the Appendix for an explanation regarding the above expression for  $f_{\text{B}}$ ). Equation 9 shows that an increase in the observed ligand line width will be related to the free and bound ligand line widths and the value of  $K_{\text{D}}$  for the protein–ligand complex. If it is assumed that the line width of the

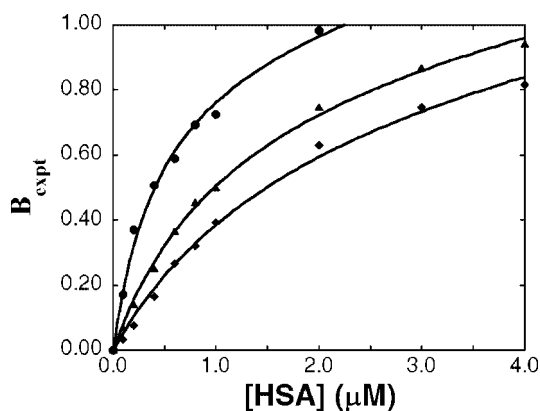
protein–ligand complex is significantly larger than that for the free ligand, the ratio of the ligand line width in the presence and absence of the protein should represent the remaining free ligand concentration, as indicated by eq 6.

This relationship assumes that there is a lack of any significant contribution of chemical or dynamic exchange to the observed change in line width. This is a reasonable assumption in the context of a high-throughput NMR screen against a single protein target. First, the initial chemical leads tend to be weak binders in the fast exchange regime, where the line width change of the ligand will be dominated by the line width of the protein. Second, biologically relevant binders will interact with the same or similar binding sites on the protein. Under these circumstances, the ligand may experience a relatively constant contribution of chemical and dynamic line-broadening. Thus, the minimal contribution of line width from exchange processes should not affect the relative ranking of the ligand binding affinities that are obtained when using such an experimental approach.

The validity of this method for high-throughput screening by NMR was examined by using twelve ligands with previously determined binding affinities to HSA.<sup>29,35–38</sup> These ligands were used to examine the relationship between

**Table 1.** Comparison of  $K_D$  Values Determined by NMR and Reported in the Literature

ligand	literature $K_D$ ( $\mu\text{M}$ )	line width (Hz)	$c$	measured $K_D$ ( $\mu\text{M}$ )
ibuprofen	0.3 <sup>65</sup> 0.33 <sup>60</sup> 0.37 <sup>64</sup> 0.5 <sup>60</sup> 0.52 <sup>49</sup> 1.0 <sup>62</sup> 1.25 <sup>45</sup> 1.26 <sup>55</sup> 1.74 <sup>56</sup> 1.89 <sup>48</sup> 2.08 <sup>45</sup> 2.8 <sup>50</sup> 4.76 <sup>56</sup> 5.56 <sup>50</sup> 5.68 <sup>53</sup> 8.33 <sup>48</sup> 7.17 <sup>44</sup> 18.2 <sup>65</sup> 23.81 <sup>35</sup> 25.64 <sup>35</sup>	2.3 ± 0.2	41.5	0.5 ± 1.0
naproxen	0.83 <sup>57</sup> 1.25 <sup>62</sup> 7.09 <sup>54</sup> 10.6 <sup>61</sup> 23.7 <sup>59</sup>	1.8 ± 0.6	51.3	0.7 ± 1.2
clofibrate	1.32 <sup>62</sup>	1.7 ± 0.1	54.3	1.7 ± 3.4
bromophenol blue	0.67 <sup>58</sup> 2.04 <sup>67</sup>	2.5 ± 0.4	37.8	3.0 ± 2.3
furosimide	5.26 <sup>51</sup> 52.63 <sup>43</sup>	1.5 ± 0.8	57.6	3.4 ± 3.0
warfarin	1.61 <sup>54</sup> 2.17 <sup>52</sup> 2.27 <sup>52</sup> 2.94 <sup>51</sup> 3.03 <sup>52</sup> 3.4 <sup>46</sup> 3.7 <sup>61</sup> 3.85 <sup>47</sup> 4.76 <sup>52</sup> 5.3 <sup>46</sup> 6.8 <sup>46</sup>	2.3 ± 0.9	41.7	4.0 ± 2.8
phenylbutazone	0.67 <sup>51</sup> 1.43 <sup>29</sup> 1.9 <sup>46</sup> 5.43 <sup>47</sup> 8.4 <sup>46</sup> 11 <sup>46</sup> 15.13 <sup>49</sup>	3.7 ± 0.6	25.2	6.5 ± 2.9
salicylate	5.26 <sup>51</sup> 15.15 <sup>52</sup> 32.15 <sup>52</sup> 35.71 <sup>52</sup> 141 <sup>61</sup>	1.4 ± 0.8	63.6	7.2 ± 2.9
bromocresol green	0.63 <sup>63</sup> 1.43 <sup>58</sup>	2.7 ± 0.3	35.1	7.4 ± 2.1
tolbutamide	4.5 <sup>36</sup> 25 <sup>51</sup> 31.25 <sup>54</sup>	2.7 ± 0.4	34.9	10.2 ± 1.2
phenol red	1.3 <sup>37</sup> 35.7 <sup>58</sup>	1.6 ± 0.5	58.7	36.8 ± 6.5
phenytoin	50 <sup>35</sup> 58.8 <sup>35</sup> 62.5 <sup>35</sup> 71.43 <sup>66</sup> 96.15 <sup>35</sup> 111 <sup>35</sup> 153.85 <sup>35</sup> 211 <sup>35</sup> 244 <sup>35</sup> 568.2 <sup>35</sup> 1342.3 <sup>35</sup>	2.0 ± 0.6	46.8	131.6 ± 12.5

**Figure 2.** Experimental fractional occupancy ( $B$ ) for naproxen (■), tolbutamide (▲), and phenol red (◆) versus the total concentration of HSA. The best-fit lines were obtained using eq 8. The  $r^2$  values for these best-fit lines are given in the text, and the  $K_D$  values that were obtained from these lines are provided in Table 1.

the estimated values for  $K_D$  and the relative ratios of the NMR peak height. Samples containing 20  $\mu\text{M}$  of any given ligand were titrated with solutions that contained 0–4  $\mu\text{M}$  HSA to develop full binding curves for each of the twelve ligands. As a control, two suspected nonbinding ligands (i.e., choline bromide and uridine-5'-monophosphate) were also screened in the presence of HSA with no observable decrease in signal (data not shown). The  $K_D$  values that were obtained by this method (see Table 1) were experimentally determined by directly fitting the resulting binding curve of each ligand to eq 8. These fits gave a sum of residuals squared that ranged between 0.977 and 0.998 over the ten concentrations of HSA that were tested. Figure 2 shows the results that were obtained for three of the tested ligands, which have previously reported dissociation equilibrium constants that ranged from 0.7 to 36.8  $\mu\text{M}$ . These figures and the corresponding fits illustrate the ability of this approach to be used with ligands that have weak-to-moderate strength binding to proteins such as HSA.

**Covariance of  $K_D$  and the NMR Line Width Ratio ( $c$ ).** Ideally, the dissociation equilibrium constant ( $K_D$ ) and the NMR line width ratio ( $c$ ) could be simultaneously derived by fitting eq 6 to the experimental NMR binding curves. Unfortunately,  $K_D$  and  $c$  are completely covariant. This requires an approximation for  $c$  to calculate  $K_D$  from the NMR binding curves. The line width of a protein ( $\nu_p$ ) may provide a lower estimate of  $\nu_B$  if it is assumed that  $\nu_B$  is

dominated by the protein line width ( $\nu_p$ ). Estimations of  $\nu_p$  can be made from the correlation time ( $\tau_c$ ) of the protein by using the intramolecular dipole–dipole relaxation rate constant ( $T_2^{-1}$ ).<sup>39</sup>

$$T_2^{-1} = \frac{3}{20} b^2 \{3J(0) + 5J(\omega_0) + 2J(2\omega_0)\} \quad (10)$$

where

$$b = -\frac{\mu_0 \hbar \gamma^2}{4\pi r^3}, \quad J(\omega) = \frac{\tau_c}{1 + \omega^2 \tau_c^2} \quad \text{and} \quad \omega_0 = -yB_0 \quad (11)$$

In these equations,  $J(\omega)$  is the normalized spectral density function,  $\mu_0$  is the vacuum permeability,  $\gamma$  is the magnetogyric ratio,  $\omega$  is frequency ( $\text{rad s}^{-1}$ ),  $\hbar$  is Planck's Constant,  $B_0$  is the static magnetic field strength, and  $r$  is the hydrodynamic radius of the protein. In addition, the Stokes–Einstein equation can be used to relate  $\tau_c$  to the molecular weight (MW) for a globular protein<sup>40</sup>

$$\tau_c = \frac{4\pi\eta r^3}{3kT} \quad \text{with} \quad \tau_c \approx \rho * \frac{\text{MW}}{2400} (\text{ns}) \quad (12)$$

where  $T$  is the temperature,  $k$  is the Boltzmann constant,  $\eta$  is the viscosity of the solvent,  $r$  is the radius, and  $\rho$  is the shape constant.

The reliability of eq 12 to approximate a protein correlation time from its molecular weight is illustrated from a comparison between 27 experimental  $\tau_c$  values<sup>41,42</sup> and correlation times predicted using eq 12 (Figure 3A). A linear best-fit was obtained with an  $r^2$  of 0.81 in this case. For a high-throughput screen,  $\nu_p$  can be estimated from the molecular weight of a protein by using this approximation for  $\tau_c$  with a shape constant of 1.32 combined with eq 10 and 11. The shape constant was determined by optimizing a linear fit between the experimental and predicted  $\tau_c$  values shown in Figure 3A by varying  $\rho$ . The result is an approximate correlation between  $\nu_p$  and  $\text{MW}_p$ , as shown in eq 13.

$$\nu_p = 1.26 \times \text{MW}_p \quad (13)$$

This dependency of line width on the size and shape of a protein is plotted in Figure 3B. For HSA (MW, 66 kDa), the correlation time (41 ns) has previously been measured using time-resolved fluorescence spectroscopy.<sup>32</sup> This correlation time was used to calculate the value used for  $\nu_p$ , which was 94.2 Hz.

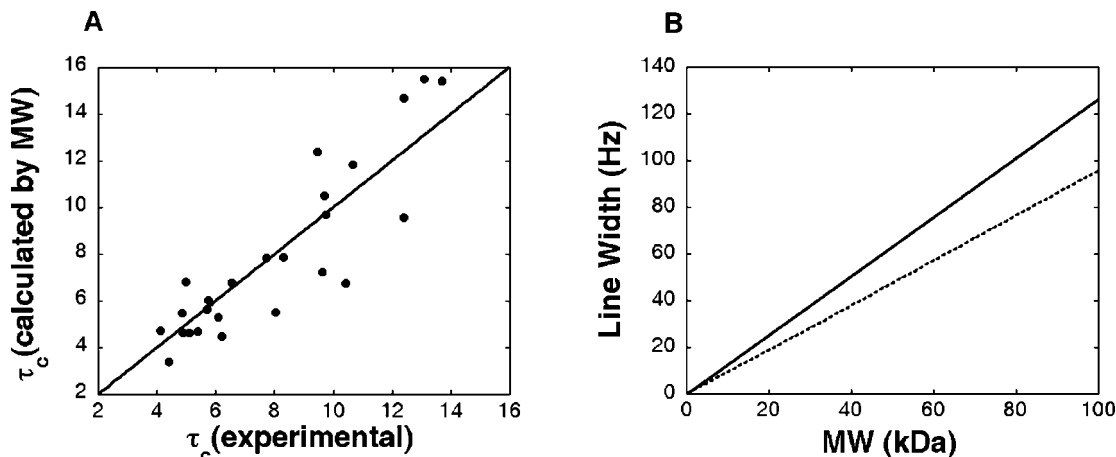


**Figure 3.** (A) Comparison of 27 experimental protein correlation times determined using NMR dynamics data with correlation times predicted from protein MW using eq 12 and a shape constant of 1.32. A best-fit line is shown with a slope of 1 and an  $r^2$  of 0.81. (B) A plot of line width versus protein molecular weight based on eq 12 for spherical proteins with  $\rho = 1$  (solid line) and elliptical proteins with  $\rho = 1.32$  (dashed).

The free ligand line width ( $\nu_F$ ) can be measured directly from the NMR spectra of the free ligand using an average ligand line width. Average  $\nu_F$  values measured from the free ligand NMR spectra are reported in Table 1. However, for large and diverse chemical libraries, it may not be feasible to measure an accurate line width for each compound. Alternatively,  $\nu_F$  is generally between 1 and 2 Hz for many small molecules (MW, 500 < Da), which provides a reasonable estimate for  $\nu_F$  to calculate an average value for  $c$ .

**Sensitivity of  $K_D$  and NMR Line Width Ratio ( $c$ ).** A closer examination of eq 6 indicates that the NMR line width ratio ( $c$ ) acts as a scaling factor in the calculation of  $K_D$ , with a larger  $c$  value resulting in a proportionally larger  $K_D$  value. Unfortunately, small variations or errors in the measurement of  $\nu_F$  will result in proportionally larger variations in both  $c$  and  $K_D$ . In the context of high-throughput screening by NMR, an incorrect estimate of  $c$  will result in a systematic underestimation or overestimation of  $K_D$ . However, the relative ranking of the ligand binding affinities will be maintained. In addition, a lower limit to  $c$  is inherently defined by eq 6.

**Comparison of Estimated  $K_D$  Values with Literature Values.** Table 1 shows the dissociation equilibrium constants that were measured for twelve ligands known to bind HSA by using the 1D  $^1\text{H}$  NMR line-broadening method that is described in this report. Previously reported  $K_D$  values from the literature are also listed for these twelve ligands.<sup>35–37,43–67</sup> In general, there is good agreement between the  $K_D$  values that were estimated by NMR and those values reported in the literature. Variations in temperature, pH, or buffer conditions may partly explain the range of  $K_D$  values observed in the literature. There may have also been differences in the fatty acid content of the HSA preparations, which can affect the reported  $K_D$  values. Thus, 1D  $^1\text{H}$  NMR line-broadening measurements appear to provide reliable preliminary estimates for binding affinities as part of a high-throughput screening assay.

One limitation of the model that was used for this analysis is the assumption of only a single site interaction between

the ligand and protein. There are many cases for which multisite binding or other effects (e.g., allosteric interactions) are present that give rise to more complex binding models.<sup>3,29,35,39</sup> Multisite binding also contributes to the relatively large range of  $K_D$  values reported in the literature for HSA ligands. In these situations, the  $K_D$  values listed in Table 1 (for both the NMR and literature results) should be regarded as weighted averages and as measures of the global affinity for a particular ligand with HSA. This averaging effect may be more pronounced for the NMR method than for other techniques because of the practical limit in ligand concentration that could be used to provide a measurable signal. There is also a practical limit to the number of concentrations and data points that could be sampled to give a binding curve. This effect may explain why the NMR-derived  $K_D$  values tend to be lower than the literature values, because the use of higher concentrations for the NMR studies would give a higher weight and likelihood to the detection of weaker interactions between the ligand and protein.

A number of other practical limitations also need to be considered in the use of NMR for these binding studies. For instance, the NMR resonances that are specifically involved with protein binding have been shown to exhibit the most dramatic changes in line width.<sup>27,28</sup> Therefore, there are inherent errors caused by summing all peak height and selectively excluding ligand peaks due to an overlap with buffer and protein resonances. In addition, errors in the measurement of peak height might arise at lower ligand concentrations because of the difficulty of accurately identifying and selecting peaks under these conditions. The result could be either a low or high estimate for  $K_D$ , depending on the disparity in line width changes and on which peaks are excluded. Using overlapping peaks would introduce an alternative error because the observed height is the sum of multiple peaks that cannot be easily deconvoluted. Also, the analysis of hundreds to thousands of NMR spectra in a high-throughput screening assay precludes a manual inspection to selectively determine which peaks to include or exclude.

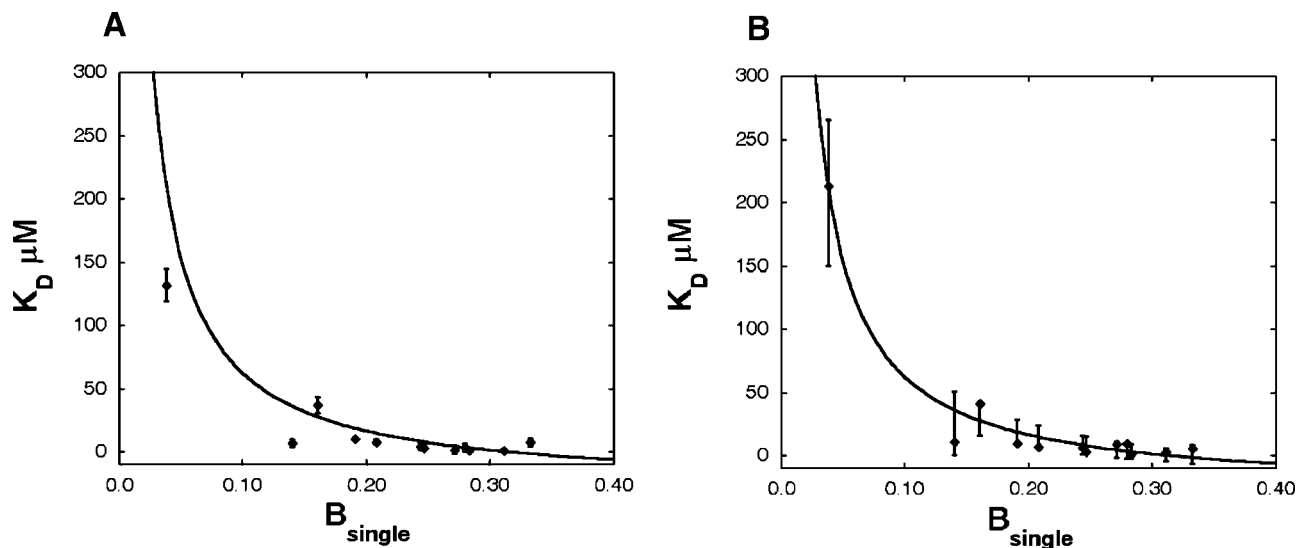


**Figure 4.** Use of NMR in a single-point binding analysis for several small-molecule ligands with known interactions with the protein HSA. The curves in panels A and B represent the ideal single-point  $K_D$  values calculated from eq 7 with  $0.2 \mu\text{M}$  HSA and an average  $c$  value of  $45.7 \pm 11.6$ . (A) The  $K_D$  values and errors reported in Table 1 are superimposed on the ideal fit. The  $K_D$  values are based on the best-fit to eq 8 using the  $c$  values determined for each individual compound. (B) The  $K_D$  for each compound was recalculated based on the best-fit to eq 8 using the  $c$  values from Table 1. The error bars in B represent the range of  $K_D$  values measured from the range of  $c$  values with the error in the free ligand line width,  $\nu_F$ , propagated.

**Estimating  $K_D$  Based on Single-Point 1D  $^1\text{H}$  NMR Line-Broadening Measurements.** Since NMR-based screens are a common component of the drug discovery process in the pharmaceutical industry, single-point estimates of ligand binding affinities could be an extremely valuable tool to initially rank and prioritize chemical leads. During the iterative drug optimization process, it is typical to focus on a small set (i.e., 3–5 compounds) of structurally distinct chemical classes that are amenable to synthetic modification and that exhibit druglike characteristics.<sup>68</sup> For this work, an NMR screen could be used to verify the presence of a specific and biologically relevant interaction involving a protein target and to rank the relative binding affinity of the screened ligands to simplify the selection of promising lead compounds. This approach was illustrated in this study by simulating NMR high-throughput screening results for the twelve compounds that were used in the previous binding study.

First, using an average  $c$  value of  $45.7 \pm 11.6$  and an HSA concentration of  $0.2 \mu\text{M}$ , single-point  $K_D$  values were calculated for a range of  $B_{\text{single}}$  values using eq 7. The result of this calculation are shown in Figure 4. Superimposed on the single point curve in Figure 4A are the  $K_D$  values reported in Table 1 plotted versus the experimental  $B$  values at  $0.2 \mu\text{M}$  HSA. Superimposed on the single point curve in Figure 4B are the  $K_D$  values from Table 1, where the corresponding  $c$  values were used to determine a best-fit to eq 8. This represents the typical protocol that would be used in a high-throughput screen and shows that an average value of  $c$  is acceptable for use when individual estimates of  $c$  may not be practical. A comparison of Figure 4B with the theoretical curve based on eq 7 indicates that the single-point method can provide a reasonable approximation for  $K_D$ .

For the twelve compounds that were considered in Figure 4B, all compounds gave single-point estimates that agreed within a range of one standard deviation over the range of

binding affinities and concentrations that were tested. All twelve compounds had experimental and single-point estimates for  $K_D$  that agreed within two standard deviations. A higher deviation was observed in Figure 4A for ligands with higher  $K_D$  values. This occurs because of differences between the individual  $c$  values and the average  $c$  values. Also, eq 8 is more sensitive to small changes in  $c$  at these high  $K_D$  values. This occurs because, at high  $K_D$  values, vanishingly small differences in NMR intensities correspond to large differences in  $K_D$ . In other words, this method is reaching a practical limit of detection since  $K_D$  rapidly approaches infinity as NMR peak height changes approach zero.

The relative ranking of the  $K_D$  values were also the same for results that were obtained by the single-point calculations or the full titration method. These results indicate that the single-point method can, at least in cases such as these, provide a preliminary estimate of  $K_D$  values and binding affinities that can be used in the context of a high-throughput screening assay. At a minimum, the relative changes in line width provide a rapid and efficient mechanism to prioritize NMR screening leads for further evaluation. However, it is still recommended that a more robust approach for measuring binding affinities for promising leads follow the NMR ligand affinity screen. This precaution follows, in part, from the fact that the accuracy of the  $K_D$  values that are measured from the single-point  $^1\text{H}$  NMR line-broadening experiments will be strongly dependent on having a reasonable estimate for the value of NMR-line width ratio ( $c$ ) in such a study.

## Conclusions

High-throughput NMR screening methods are commonly used to determine protein–ligand binding interactions. A methodology to estimate binding affinities and rank chemical leads from 1D  $^1\text{H}$  NMR line-broadening experiments was described in this article. A new equation was derived that allowed a dissociation equilibrium constant for protein–ligand



binding to be determined from a single-point NMR peak height change. This approach assumes a single binding-site interaction that is in the NMR fast-exchange regime with uniform changes in compound linewidths. These are reasonable assumptions during the initial stages of a drug discovery effort, where typical lead compounds will have weak micro- to millimolar dissociation constants. The technique was demonstrated by measurement of the dissociation equilibrium constants for twelve compounds that bind to HSA. Although this approach does have a number of practical limitations that must be considered, a reasonable correlation was observed between the binding affinities that were estimated by NMR and previously reported literature values for the tested compounds. Such information should be quite useful if the intent is to use the 1D  $^1\text{H}$  NMR line-broadening method as part of high-throughput screening to rank the binding affinities for ligands to a given protein. For instance, this approach could be used to prioritize chemical leads during a drug discovery process before these leads undergo further evaluation by secondary assays that can provide a more robust measurement of dissociation equilibrium constants. This technique is also a general approach that can be applied to various systems for high-throughput screening.

**Acknowledgment.** This work was supported by grants from the Nebraska Tobacco Settlement Biomedical Research Development Funds, the Nebraska Research Council, and the John C. and Nettie V. David Memorial Trust Fund. Work by D.S.H. was funded by the NIH under Grant R01 GM044931. Research was performed in facilities renovated with support from the NIH under Grant RR015468-01. We would like to thank Jennifer Copeland and Bo Zhang for their assistance in preparing the manuscript.

L	small-molecule ligand
$[\text{L}]_{\text{T}}$	total ligand concentration
$[\text{L}]_{\text{F}}$	free ligand concentration
P	protein target
$[\text{P}]_{\text{T}}$	total protein concentration
$[\text{P}]_{\text{F}}$	free protein concentration
$[\text{PL}]$	protein–ligand complex concentration
$I_{\text{B}}$	NMR peak height of bound ligand
$I_{\text{F}}$	NMR peak height of free ligand
$K_{\text{D}}$	dissociation equilibrium constant for a protein–ligand complex
$c$	NMR line width ratio constant
$B$	NMR signal response dependent on fraction of bound ligand
$B_{\text{single}}$	NMR signal response dependent on fraction of bound ligand at a single $[\text{P}]_{\text{T}}$ and $[\text{L}]_{\text{T}}$
$\nu_{\text{F}}$	line width of the free ligand
$\nu_{\text{B}}$	line width of the bound protein–ligand complex
$\nu_{\text{P}}$	line width of the protein
$\nu_{\text{obs}}$	observed line width change upon addition of protein or ligand
$f_{\text{B}}$	fraction bound complex in solution
$f_{\text{F}}$	fraction of free ligand in solution

$T_2^{-1}$	dipole–dipole relaxation constant
$\tau_c$	correlation time
$J(\omega)$	normalized density function of $T_2^{-1}$
$B_0$	static magnetic field strength
$\omega_0$	Larmor frequency
$\text{MW}_{\text{P}}$	molecular weight of a protein target

## Appendix

The binding of a protein (P) with a single small ligand (L) can be represented by the following reaction:



The dissociation equilibrium constant for this system is described by the expression in eq A2, where the concentrations  $[\text{P}]_{\text{F}}$ ,  $[\text{L}]_{\text{F}}$  and  $[\text{PL}]$  represent the concentration of free protein, free ligand, and protein–ligand complex, respectively.

$$K_{\text{D}} = \frac{[\text{P}]_{\text{F}}[\text{L}]_{\text{F}}}{[\text{PL}]} \quad (\text{A2})$$

On the basis of the mass balance, eq A3 can be used to express  $[\text{L}]_{\text{F}}$  and  $[\text{PL}]$  in terms of the total ligand concentration and other concentrations in this system.

$$[\text{P}]_{\text{T}} - [\text{P}]_{\text{F}} = [\text{PL}] = [\text{L}]_{\text{T}} - [\text{L}]_{\text{F}} \Rightarrow [\text{L}]_{\text{F}} = [\text{L}]_{\text{T}} - [\text{P}]_{\text{T}} + [\text{P}]_{\text{F}} \quad (\text{A3})$$

Substitution of these relationships into eq A2 gives eq A4.

$$K_{\text{D}} = \frac{[\text{P}]_{\text{F}}([\text{L}]_{\text{T}} - [\text{P}]_{\text{T}} + [\text{P}]_{\text{F}})}{[\text{P}]_{\text{T}} - [\text{P}]_{\text{F}}} \quad (\text{A4})$$

Eq A4 can now be rearranged into the following form

$$K_{\text{D}}([\text{P}]_{\text{T}} - [\text{P}]_{\text{F}}) = [\text{P}]_{\text{F}}([\text{L}]_{\text{T}} - [\text{P}]_{\text{T}} + [\text{P}]_{\text{F}}) \Rightarrow [\text{P}]_{\text{F}}^2 + ([\text{L}]_{\text{T}} - [\text{P}]_{\text{T}} + K_{\text{D}})[\text{P}]_{\text{F}} - K_{\text{D}}[\text{P}]_{\text{T}} = 0 \quad (\text{A5})$$

which makes it possible to solve for  $[\text{P}]_{\text{F}}$  by using the quadratic formula, as indicated in eq A6, where only the positive root has any meaning in a real protein–ligand system.

$$[\text{P}]_{\text{F}} = \frac{-([\text{L}]_{\text{T}} - [\text{P}]_{\text{T}} + K_{\text{D}}) \pm \sqrt{([\text{L}]_{\text{T}} - [\text{P}]_{\text{T}} + K_{\text{D}})^2 + 4K_{\text{D}}[\text{P}]_{\text{T}}}}{2} \quad (\text{A6})$$

The bound fraction of ligand  $f_{\text{B}}$  is next defined as given in eq A7.

$$f_{\text{B}} = \frac{[\text{PL}]}{[\text{PL}] + [\text{L}]_{\text{F}}} = \frac{1}{1 + \frac{K_{\text{D}}}{[\text{P}]_{\text{F}}}} \quad (\text{A7})$$

If we substitute the positive root of eq A6 into eq A7, the result is eq A8.

$$f_B = \frac{1}{1 + \frac{2K_D}{-([L]_T - [P]_T + K_D) + \sqrt{([L]_T - [P]_T + K_D)^2 + 4K_D[P]_T}}} = \frac{1}{1 + \left(\frac{2K_D}{([L]_T - [P]_T + K_D)}\right) \left(\sqrt{1 + \frac{4K_D[P]_T}{([L]_T - [P]_T + K_D)^2}} - 1\right)^{-1}} \quad (\text{A8})$$

A further simplification of eq 8 can be accomplished by expanding the square root as a power series where  $x = 4K_D[P]_T/([L]_T - [P]_T + K_D)^2$  about  $x = 0$ . This approach is valid as long as the ligand is in considerable excess relative to the protein. The power series that is used here is shown below.

$$\sqrt{1+x} = 1 + \frac{x}{2} - \frac{x^2}{8} + \dots \quad (\text{A9})$$

If eq A9 is truncated at the second term, this allows the square root term in eq A8 to be written in the approximate form that is given in eq A10.

$$\sqrt{1 + \frac{4K_D[P]_T}{([L]_T - [P]_T + K_D)^2}} \approx 1 + \frac{2K_D[P]_T}{([L]_T - [P]_T + K_D)^2} \quad (\text{A10})$$

The overall result of this simplification is that eq A8 converts to the expression shown below, there the fraction of bound ligand  $f_B$  is now described in terms of only  $K_D$ , the total ligand concentration, and the total protein concentration.

$$f_B \approx \frac{1}{1 + \frac{2K_D[P]_T}{([L]_T - [P]_T + K_D)^2}} = \frac{[P]_T}{([L]_T + K_D)} \quad (\text{A11})$$

If it is assumed that the observed free and bound NMR-linewidths are represented by  $\nu_F$  and  $\nu_B$ , respectively, and that exchange occurs between free and bound states, the general solution to the NMR line shape is bi-Lorentzian. In the slow limit, the spectrum is obviously just a sum of the spectra of free and bound species, weighted by their relative abundances. If exchange rates become comparable to the inverse line widths, then a conventional solution of the pair of coupled linear differential equations, including auto- and cross-relaxation terms but neglecting any chemical shift difference between the states, gives a time domain (free induction decay)

$$f(t) = c_+e_+ + c_-e_- \quad (\text{A12a})$$

with

$$e_{\pm} = \exp[(\Theta \pm \sqrt{\Delta})t] \quad (\text{A12b})$$

$$c_{\pm} = c_2 \pm \frac{c_1}{\sqrt{\Delta}} \quad (\text{A12c})$$

$$c_1 = \frac{1}{4}[(\bar{K}_{11} + 2\bar{K}_{21} - \bar{K}_{22})M_L(0) - (\bar{K}_{11} - 2\bar{K}_{12} - \bar{K}_{22})M_{PL}(0)] \quad (\text{A12d})$$

$$c_2 = \frac{1}{2}(M_L(0) + M_{PL}(0)) \quad (\text{A12e})$$

$$\Delta = \left(\frac{\bar{K}_{11} - \bar{K}_{22}}{2}\right)^2 + \bar{K}_{12}\bar{K}_{21} \quad (\text{A12f})$$

$$K_{11} = -\frac{1}{T_{2,f}} - k_1[P] \quad (\text{A12g})$$

$$K_{22} = -\frac{1}{T_{2,b}} - k_{-1} \quad (\text{A12h})$$

$$K_{12} = k_{-1} \quad (\text{A12i})$$

$$K_{21} = k_1[P] \quad (\text{A12j})$$

where  $M_L$  and  $M_{PL}$  are the magnetization of the free and bound species, respectively. In the fast exchange limit, the solution is still formally biexponential, but the coefficient  $c_-$  goes to zero, and the free induction decay signal, normalized to unity at zero time, becomes the following

$$f(t) = \exp\left(-\frac{1}{T_{2,f}}\left\{\frac{[L]}{([L] + [PL])}\right\} - \frac{1}{T_{2,b}}\left\{\frac{[PL]}{([L] + [PL])}\right\}\right) = \exp\left(-\frac{f_f}{T_{2,f}} - \frac{f_b}{T_{2,b}}\right) \quad (\text{A13})$$

After, Fourier transforming, the fast exchange NMR signal height can be written as shown in eq A14

$$I_B = \frac{I_F \nu_F}{f_F \nu_F + f_B \nu_B} \quad (\text{A14})$$

where  $I_F$  is the height of the ligand signal in the absence of protein and  $I_B$  is the observed peak height of the bound complex. This is exactly the same as the height of the free ligand signal in extreme slow exchange! Rearranging eq A14 explains the observed decrease in NMR peak signal for a free small-molecule ligand upon its binding to a protein. The relative ratio of NMR peak height ( $I_B/I_F$ ) is now in terms of the fraction of free ligand ( $f_F$ ) and the fraction of bound ligand ( $f_B$ ) and is dependent on the observed increase in NMR line width upon the binding of a ligand to a protein.

$$\begin{aligned} 1 - \frac{I_B}{I_F} &= 1 - \frac{\nu_F}{f_F \nu_F + f_B \nu_B} \\ &= 1 - \frac{1}{f_F + (f_B \nu_B / \nu_F)} \\ &= 1 - \frac{1}{1 - f_B + (f_B \nu_B / \nu_F)} \\ &= 1 - \frac{1}{1 + f_B \left(\frac{\nu_B}{\nu_F} - 1\right)} \end{aligned} \quad (\text{A15})$$

Inserting A11 into A15 provides a measure of the dissociation equilibrium constant for the protein–ligand complex by relating the fraction of bound ligand to the observed change in NMR peak height.

$$\begin{aligned}
 B &= 1 - \frac{I_B}{I_F} \\
 &= 1 - \frac{1}{1 + \frac{[P]_T}{[L]_T + K_D} \left( \frac{\nu_B}{\nu_F} - 1 \right)} \\
 &= 1 - \frac{1}{1 + \frac{c[P]_T}{[L]_T + K_D}} \quad \text{where } c \\
 &= \frac{\nu_B}{\nu_F} - 1 \quad (\text{A16})
 \end{aligned}$$

The NMR-line width ratio,  $c$ , is then measured by using the free ligand NMR spectrum and by assuming that the line width of the bound complex approximates the line width of the protein.

## References and Notes

- Zartler, E. R.; Shapiro, M. J. *Curr. Pharm. Des.* **2006**, *12* (31), 3963.
- Fejzo, J.; Lepre, C. A.; Peng, J. W.; Bemis, G. W.; Ajay Murcko, M. A.; Moore, J. M. *Chem. Biol.* **1999**, *6*, 755–769.
- Hajduk, P. J.; Olejniczak, E. T.; Fesik, S. W. *J. Am. Chem. Soc.* **1997**, *119*, 12257–12261.
- Shuker, S. B.; Hajduk, P. J.; Meadow, R. P.; Feisk, S. W. *Science* **1996**, *274* (5292), 1531–1534.
- Wagner, G.; Hyberts, S. G.; Havel, T. F. *Annu. Rev. Biophys. Biomol. Struct.* **1992**, *21*, 167–198.
- Vanwetswinkel, S.; Heetebrij, R. J.; Duynhoven, J. v.; Hollander, J. G.; Filippov, D. V.; Hajduk, P.; Siegal, G. *Chem. Biol.* **2005**, *12*, 207–216.
- Peng, J. W.; Moore, J.; Abdul-Manan, N. *Prog. Nucl. Magn. Reson. Spectrosc.* **2004**, *44*, 225–256.
- Zartler, E. R.; Hanson, J.; Jones, B. E.; Kline, A. D.; Martin, G.; Mo, H.; Shapiro, M. J.; Wang, R.; Wu, H.; Yan, J. *J. Am. Chem. Soc.* **2003**, *125* (36), 10941–10946.
- Sem, D. S.; Bertolalet, B.; Baker, B.; Chang, E.; Costache, A. D.; Coutts, S.; Dong, Q.; Hansen, M.; Hong, V.; Huang, X.; Jack, R. M.; Kho, R.; Lang, H.; Ma, C.-T.; Meininger, D.; Pellicchia, M.; Pierre, F.; Villar, H.; Yu, L. *Chem. Biol.* **2004**, *11* (2), 185–194.
- Moy, F. J.; Haraki, K.; Mobilio, D.; Walker, G.; Powers, R. *Anal. Chem.* **2001**, *73* (3), 571–581.
- Mercier, K. A.; Baran, M.; Ramanathan, V.; Revesz, P.; Xiao, R.; Montelione, G. T.; Powers, R. *J. Am. Chem. Soc.* **2006**, *128* (48), 15292–15299.
- Mercier, K. A.; Germer, K.; Powers, R. *Comb. Chem. High Throughput Screening* **2006**, *9* (7), 515–534.
- Villar, H. O.; Yan, J.; Hansen, M. R. *Curr. Opin. Chem. Biol.* **2004**, *8*, 387–391.
- Fejzo, J.; Lepre, C. A.; Xie, X. *Curr. Top. Med. Chem.* **2003**, *3*, 81–97.
- Johnson, E. C.; Feher, V. A.; Peng, J. W.; Moore, J. M.; Williamson, J. R. *J. Am. Chem. Soc.* **2003**, *125*, 15724–15725.
- Homans, S. W. *Angew. Chem., Int. Ed.* **2004**, *43*, 290–300.
- Wang, Y.-S.; Liu, D.; Wyss, D. F. *Magn. Reson. Chem.* **2004**, *42*, 485–489.
- Chen, A.; Shapiro, M. J. *J. Am. Chem. Soc.* **1998**, *120*, 10258–10259.
- Fielding, L. *Curr. Top. Med. Chem.* **2003**, *3*, 39–53.
- Copeland, R. A., *Enzymes: A Practical Introduction to Structure, Mechanism, Data Analysis*, 2nd ed.; Wiley-VCH: New York, 2000; p 397.
- Dalvit, C.; Ardini, E.; Flocco, M.; Fogliatto, G. P.; Mongelli, N.; Veronesi, M. *J. Am. Chem. Soc.* **2004**, *125* (47), 14620–14625.
- Tengel, T.; Fex, T.; Emtenas, H.; Almqvist, F.; Sethson, I.; Kihlberg, J. *Org. Biomol. Chem.* **2004**, *5*, 725–731.
- Siriwardena, A. H.; Tian, F.; Noble, S.; Prestegard, J. H. *Angew. Chem., Int. Ed.* **2002**, *41* (18), 3454–3457.
- Jahnke, W.; Floersheim, P.; Ostermeier, C.; Zhang, X.; Hemmig, R.; Hurth, K.; Uzunov, D. P. *Angew. Chem., Int. Ed.* **2002**, *41* (18), 3420–3423.
- Dalvit, C.; Flocco, M.; Knapp, S.; Mostardini, M.; Perego, R.; Stockman, B. J.; Veronesi, M.; Varasi, M. *J. Am. Chem. Soc.* **2002**, *124*, 7702–7709.
- Dalvit, C.; Flocco, M.; Stockman, B. J.; Veronesi, M. *Comb. Chem. High Throughput Screening* **2002**, *5*, 645–650.
- Fischer, J. J.; Jardetzky, O. *J. Am. Chem. Soc.* **1965**, *87* (14), 3237–3244.
- Sarrazin, M.; Sari, J. C.; Bourdeaux-Pontier, M.; Briand, C. *Mol. Pharm.* **1972**, *15*, 71–77.
- Peters, T., *All About Albumin: Biochemistry, Genetics, and Medical Applications*; Academic Press Inc.: London, 1995.
- Cavanagh, J.; Fairbrother, W. J.; Palmer, A. G., III; Skelton, N. J., *Protein NMR Spectroscopy: Principles and Practice*; Academic Press: San Diego, 1996; p 587.
- Packer, K. J.; Thomlinson, D. J. *Trans. Faraday Soc.* **1971**, *67*, 1302–1314.
- Helms, M. K.; Petersen, C. E.; Bhagavan, N. V.; Jameson, D. M. *FEBS Lett.* **1997**, *408* (1), 67–70.
- Zartler, E. R.; Yan, J.; Mo, H.; Kline, A. D.; Shapiro, M. J. *Curr. Top. Med. Chem.* **2003**, *3*, 25–37.
- Coles, M.; Heller, M.; Kessler, H. *Drug Discovery Today* **2003**, *8* (17), 803–810.
- Chen, J.; Ohnmacht, C.; Hage, D. S. *J. Chromatogr. B: Anal. Technol. Biomed. Life Sci.* **2004**, *809* (1), 137–145.
- Kurtzhals, P.; Havelund, S.; Joanassen, I.; Markussen, J. *J. Pharm. Sci.* **1997**, *86* (12), 1365–1368.
- Sengupta, A.; Hage, D. S. *Anal. Chem.* **1999**, *71* (17), 3821–3827.
- Kragh-Hansen, U.; Chuang, V. T. G.; Otagiri, M. *Bio. Pharm. Bull.* **2002**, *25* (6), 695–704.
- Levitt, M. H., *Spin Dynamics, Basics of Nuclear Magnetic Resonance*; John Wiley & Sons: Chichester, U.K., 2001; p 520–537.
- Cantor, C. R.; Schimmel, P. R., *Biophysical Chemistry Part II: Techniques for the Study of Biological Structure and Function*; W. H. Freeman and Co: San Francisco, CA, 1980; p 461.
- Bernardo, P.; Garcia de la Torre, J.; Pons, M. *J. Biomol. NMR* **2002**, *23* (2), 139–150.
- Garcia de la Torre, J.; Huertas, M. L.; Carrasco, B. *J. Magn. Reson.* **2000**, *147* (1), 138–146.
- Ascenzi, P.; Bocedi, A.; Notari, S.; Menegatti, E.; Fasano, M. *Biochem. Biophys. Res. Commun.* **2005**, *334* (2), 481–486.
- Ascoli, G.; Bertucci, C.; Salvadori, P. *J. Pharm. Sci.* **1995**, *84* (6), 737–741.
- Cheruvallath, V. K.; Riley, C. M.; Narayanan, S. R.; Lindenbaum, S.; Perrin, J. H. *J. Pharm. Biomed. Anal.* **1997**, *15* (11), 1719–1724.
- Epps, D. E.; Raub, T. J.; Kezdy, F. J. *Anal. Biochem.* **1995**, *227* (2), 342–350.
- Hage, D. S. *J. Chromatogr. B: Ana. Technol. Biomed. Life Sci.* **2002**, *768* (1), 3–30.
- Hage, D. S.; Noctor, T. A.; Wainer, I. W. *J. Chromatogr. A* **1995**, *693* (1), 23–32.
- Hollosy, F.; Valko, K.; Hersey, A.; Nunhuck, S.; Keri, G.; Bevan, C. *J. Med. Chem.* **2006**, *49* (24), 6958–6971.
- Itoh, T.; Saura, Y.; Tsuda, Y.; Yamada, H. *Chirality* **1997**, *9* (7), 643–649.

- (51) Kragh-Hansen, U.; Chuang, V. T.; Otagiri, M. *Biol. Pharm. Bull.* **2002**, 25 (6), 695–704.
- (52) Lagercrantz, C.; Larsson, T. *Biochem. J.* **1983**, 213 (2), 387–390.
- (53) Lockwood, G. F.; Albert, K. S.; Szpunar, G. J.; Wagner, J. G. *J. Pharmacokinet. Biopharm.* **1983**, 11 (5), 469–482.
- (54) Margarita Valero, B. E.; Pelaez, R.; Rodriguez, L. J. *J. Inclusion Phenom.* **2004**, 48, 157–163.
- (55) Montero, M. T. E. J.; Valls, O. *Int. J. Pharm.* **1990**, 62 (1), 21–25.
- (56) Paliwal, J. K.; Smith, D. E.; Cox, S. R.; Berardi, R. R.; Dunn-Kucharski, V. A.; Elta, G. H. *J. Pharmacokinet. Biopharm.* **1993**, 21 (2), 145–161.
- (57) Patonay, G.; Salon, J.; Sowell, J.; Strekowski, L. *Molecules* **2004**, 9 (3), 40–49.
- (58) Peters, T. *All About Albumin: Biochemistry, Genetics, and Medical Applications*; Academic Press: San Diego, CA, 1996, Chapter 3.
- (59) Pirnau, A. a B. M. *Rom. J. Biophys.* **2008**, 18 (1), 49–55.
- (60) Rahman, M. H.; Maruyama, T.; Okada, T.; Imai, T.; Otagiri, M. *Biochem. Pharmacol.* **1993**, 46 (10), 1733–1740.
- (61) Rich, R. L.; Day, Y. S.; Morton, T. A.; Myszka, D. G. *Anal. Biochem.* **2001**, 296 (2), 197–207.
- (62) Sowell, J.; Mason, J. C.; Strekowski, L.; Patonay, G. *Electrophoresis* **2001**, 22 (12), 2512–2517.
- (63) Trivedi, V. D.; Saxena, I.; Siddiqui, M. U.; Qasim, M. A. *Biochem. Mol. Biol. Int.* **1997**, 43 (1), 1–8.
- (64) Whitlam, J. B.; Crooks, M. J.; Brown, K. F.; Pedersen, P. V. *Biochem. Pharmacol.* **1979**, 28 (5), 675–678.
- (65) Yamasaki, K.; Rahman, M. H.; Tsutsumi, Y.; Maruyama, T.; Ahmed, S.; Kragh-Hansen, U.; Otagiri, M. *AAPS Pharm-SciTech* **2000**, 1 (2), E12.
- (66) Chen, J.; Hage David, S. *Nat. Biotechnol.* **2004**, 22 (11), 1445–1448.
- (67) Trivedi, V. D. *Ital. J. Biochem.* **1997**, 46 (2), 67–73.
- (68) Hajduk, P.; Betz, S. F.; Mack, J.; Ruan, X.; Towne, D. L.; Lerner, C. G.; Beutel, B. A.; Fesik, S. W. *J. Biomol. Screening* **2002**, 7 (5), 429.

CC800122M